PROCEEDINGS OF SCIENCE

On Why the 10-TeV Cosmic Ray Bump Originates in the Local Interstellar Medium

M.A. Malkov,[a,*] P.H. Diamond,[a] M. Cao[a] and I.V. Moskalenko[b]

[a] *Department of Physics and CASS, University of California San Diego, La Jolla, CA 92093, USA*

[b] *Hansen Experimental Physics Laboratory and Kavli Institute for Particle Astrophysics and Cosmology, Stanford University, Stanford, CA 94305, USA*

E-mail: mmalkov@ucsd.edu

Recent measurements of primary and secondary CR spectra, their arrival directions, and our improved knowledge of the magnetic field geometry around the heliosphere allow us to set a bound on the distance beyond which a puzzling 10-TeV "bump" *cannot* originate. The sharpness of the spectral breaks associated with the bump, the abrupt change of the CR intensity across the local magnetic equator (90° pitch angle), and the similarity between the primary and secondary CR spectral patterns point to a local reacceleration of the bump particles out of the background CRs. We argue that a nearby shock may generate such a bump by increasing the rigidity of the preexisting CRs below 50 TV by a mere factor of ∼1.5. Reaccelerated particles below ∼0.5 TV are convected with the interstellar medium flow and do not reach the Sun, thus creating the bump. This single universal process is responsible for the observed spectra of all CR species in the rigidity range below 100 TV. We propose that one viable candidate is the system of shocks associated with ϵ Eridani star at 3.2 pc of the Sun, which is well aligned with the direction of the local magnetic field. Other shocks, such as old supernova shells, may produce a similar effect. We provide a simple formula that reproduces the spectra of all CR species with only three parameters uniquely derived from the CR proton data. We show how our formalism predicts helium and carbon spectra and the B/C ratio.

38th International Cosmic Ray Conference (ICRC2023)
26 July - 3 August, 2023
Nagoya, Japan

ICRC2023
38th International Cosmic Ray Conference
The Astroparticle Physics Conference

*Speaker

PoS(ICRC2023)143

1. Introduction

Sources of cosmic rays (**CR**s) are scattered across the Galaxy. After propagation to the Earth, accompanied by a turbulent reacceleration in stochastic magnetic fields and a partial leak into intergalactic space, CRs are expected to arrive with a featureless power-law energy spectrum and a weak, $\sim 10^{-3}$, dipolar anisotropy pointing to the *inner* Galaxy. However, the new observations revealed a prominent structure in the spectra of CR primaries (so-called 10-TeV "bump") also characterized by an excess pointing to the *outer* Galaxy with a sharp step-like boundary in CR arrival directions and similar spectral anomalies in secondary CR species.

Understanding the origin of the bump offers a deeper insight into the nature of CR propagation from their sources, individual source contributions to the CR spectrum, and the structure of the local interstellar medium (ISM). Upon addressing the new challenges, we can test and improve the concept of CR origin and guide future observations.

This paper focuses on CR *reacceleration and propagation in the local* ISM ($\sim$10 pc of the Sun). An exceptional sharpness of the breaks in the spectra of CR species resolved by AMS-02, CALET, DAMPE, and ISS-CREAM orbital instruments, dictates this choice. These features persist within unprecedentedly tight error bounds. Nearby SNRs are unlikely responsible for these structures. Propagating CRs from such sources would erase fine spectral features, such as sharp breaks in rigidity spectra and small-scale angular anisotropies.

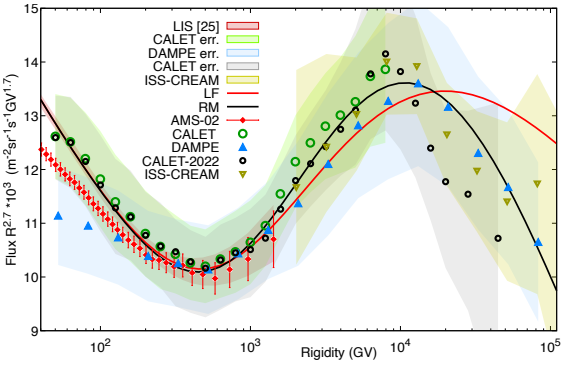

Figure 1: New prominent spectral features, shown in the 10^2–10^5 GV range for protons. Compilation of data from AMS-02 [7], CALET [5], ISS-CREAM [12], and DAMPE [9] is described in Sec.2. CALET and DAMPE data were shifted to adjust for systematic differences [16], while the ISS-CREAM data are multiplied by a factor of 1.12 for the same purpose. The lines show the local ISM spectra in two models: Red – Eq.(1) without CR losses from the magnetic flux tube, Black – the same fit with losses (see text).

On the other hand, a nearby passing star, blowing its wind against the headwind of the ISM, can make an efficient CR *reaccelerator* within 3-10 pc of the Sun. A synergy of the star's bow- and wind termination shocks, which can be supplemented by reacceleration in the stellar wind, is able to efficiently reaccelerate the preexisting CRs. Propagating then through a turbulent magnetic flux tube pointed to the Sun, the reaccelerated CRs most naturally acquire the observed spectral features by suffering energy-dependent diffusive and convective losses from the tube.

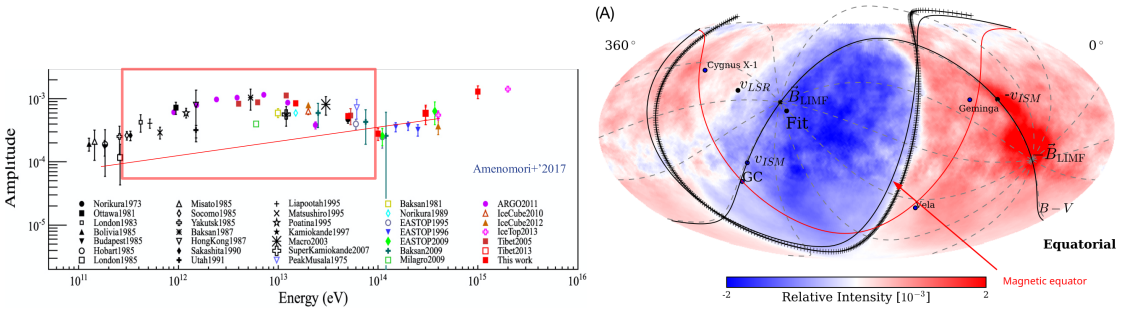

Figure 2: Left: CR anisotropy data, adopted from [8]. **Right:** CR arrival direction intensity at median primary particle energy of 10 TeV adopted from [2].

2. Observational Challenges

Energy Spectrum: The high-precision data accumulated by several new instruments [6, 7, 9, 12], Fig.1, challenge the CR acceleration and propagation theory. The figure shows a zoomed 10-TeV bump in an enhanced rigidity format with an extra $R^{2.7}$ factor. These instruments have revealed two prominent features. The deviations from the straight power law begin with a sudden flattening at ≈0.2 TV. Then, the spectrum steepens back at ≈10 TV, also very sharply. It might then return to its low-energy slope in the 100 TV range. This spectral anomaly is a challenge since the acceleration of CRs in SNR shocks and their subsequent propagation to the heliosphere was long considered scale-invariant.

Anisotropy: Anisotropy data shown in Fig.2 (left panel) is widely interpreted as almost flat in a broad energy range between 10^{11}–10^{15} eV, within uncertainties. This flatness is surprising, as the large-scale anisotropy is expected to grow with particle energy because they leave the Galaxy faster. Here we note, however, a striking coincidence between the energy range of the bump Fig.1, and the anisotropy enhancement between $\approx 2\times 10^{11} - 10^{14}$ eV, marked by a box. After that, the anisotropy briefly declines toward $\sim 10^{14}$ eV and then grows again. The enhanced anisotropy in the box area that can be primarily associated with the 10-TV rigidity bump in Fig.2 strongly suggests the flat anisotropy being composed of two independent CR sources: the background CRs with a weak but growing anisotropy, as expected, masked by a separate component comprising the bump particles.

The overall anisotropy discussed above is at a $\sim 10^{-3}$ level, corresponding to a dipole component of CRs. There is also a small-scale anisotropy at 10^{-4}, first discovered by the Milagro observatory [1]. More accurate mapping is provided by HAWC and IceCube [2], Fig.2. It shows a well-defined excess of ∼20°-wide likely associated with the CR arrival direction, and may very well be relevant to the 10-TeV CR bump.

Secondaries: Secondary species exhibit stronger spectral hardening than the primaries [7]. It takes millions of years to produce the secondaries out of the primaries in CR spallation reactions. Matching the observed breaks in secondaries with additional components produced in local sources surrounded by gas clouds requires fine-tuning.

3. How Far Away the TeV-bump May Have Formed?

Whatever the reasons for the breaks, they should form not too far from us to survive smoothing by the diffusion in momentum. Using a simple relation between the momentum diffusivity, D_p, and the spatial diffusivity κ, [18], $D_p \approx p^2 V_A^2/\kappa$, where V_A is the Alfven velocity, one can estimate the distance to the source as follows.

A sharp break spreads in momentum by $\Delta p/p \sim \sqrt{D_p t_{\rm prop}}/p \sim LV_A/\kappa$, where $L \sim \sqrt{\kappa t_{\rm prop}}$ the distance to its origin and $t_{\rm prop}$ is the propagation time. The width Δp remains small for $L \ll \kappa/V_A$. For energies above a few GeV, $\kappa \sim 10^{28}\,(p/[{\rm GeV}/c])^{\delta}\,{\rm cm}^2/{\rm s}$, $\delta = 0.3 - 0.6$, and $V_A \simeq 30$ km/s, we arrive at the following restriction $L_s \ll 1$ kpc. This restriction is rigid if the first break is as sharp as the most precise AMS-02 data suggest. More importantly, since the number density of CRs at the bump is a factor of ∼3 higher than the background CRs underneath it, these particles will likely drive Alfven waves by themselves. Simple estimates suggest a decrease in κ by at least an order of magnitude [15]. This estimate strictly limits the distance to the source to $L_s \ll 10^2$ pc. The above estimate concerned only the propagation history of the bump. Its formation in a localized source, such as an SNR, must be accompanied by an even stronger spread in momentum because of a significant reduction in κ around the source [14] and the corresponding delayed particle escape from it. We conclude that the bump must have formed not farther than a few tens of parsecs. However, the bump is unlikely to form inside or near the heliosphere.

As one of the angular CR enhancements discovered by Milagro [1] pointed to the heliotail, attempts were made at explaining it by the acceleration of CRs in the regions of a striped magnetic field in the heliotail. Other peripheral magnetic perturbations around the heliosphere have also been examined. However, the 10 TeV proton gyroradius, r_g, in the 1-3 μG field is $\sim 10^3$ au, an order of magnitude larger than the heliosphere cross-section, $R_{\rm hs}$. CR acceleration mechanisms, based, e.g., on the reconnection in the striped magnetic field in the tail, would require $R_{\rm hs} \gg r_g$, while an opposite condition is met for 10 TeV protons.

Secondary species provide another compelling argument against the nearby SNR origin of the 10-TeV bump. They exhibit a stronger spectral hardening than the primaries at the same rigidity. It indicates a rigidity-dependent modification of the spectra, possibly associated with the diffusion or diffusive reacceleration rather than the energy-per-nucleon spallation-related process. Besides, matching the Galaxy-wide spectra with the local-source-produced component requires fine-tuning the local source abundances and the rigidity dependence of the diffusion coefficient in the whole Galaxy.

The above two lines of argument imply seemingly opposite restrictions on the distance to the source of the spectral bump. On the one hand, these particles must spend a very long time in the Galaxy, thus propagating a very long distance, to process a significant "grammage" of the ISM gas. On the other hand, they somehow evade the momentum diffusion, which is inevitable in the turbulent ISM. The sharp spectral breaks in particle momentum distribution point to a relatively local origin of the breaks, while the underlying particles must have been accelerated in distant objects, most likely an ensemble of SNRs. The most natural way to reconcile this contradiction is to assume that the bump comprises *locally reaccelerated* background CRs.

4. Plausibility of the Local Origin of 10-TeV Bump

Rigidity Spectrum Suppose a stellar bow-shock, Fig.3, is moving through the ISM. At any instant, it populates a particular magnetic flux tube with CRs reaccelerated up to $R_{\max}$. They propagate primarily along the tube to a distance proportional to their rigidity. While moving further through the ISM, the star leaves a wake of flux tubes filled with reaccelerated CRs. It continues to broaden along and across the field but with the diffusivity $\kappa_\perp \ll \kappa_\parallel$.

Assume further the Sun is in the wake where only particles with rigidities $R \geq R_1$ can reach (the first break, see Fig.3). We, therefore, see the spectrum flattening at $R > R_1$. The Sun's position in the wake defines the bump parameters, as does the energy upshift due to the reacceleration (shown in the left-most spectrum in the figure). These model parameters fix the bump magnitude (factor ≈2.4 above the background) and its rigidity (∼10 TV), while the details of reacceleration are less critical. The second break at R=R_2 forms where more reaccelerated CRs reach a given position in the wake. The spectrum returns to the slope it has near the star (CR background slope if the bow shock is weak) and then to the CR background where R approaches $R_{\max}$ or the CR losses dominate.

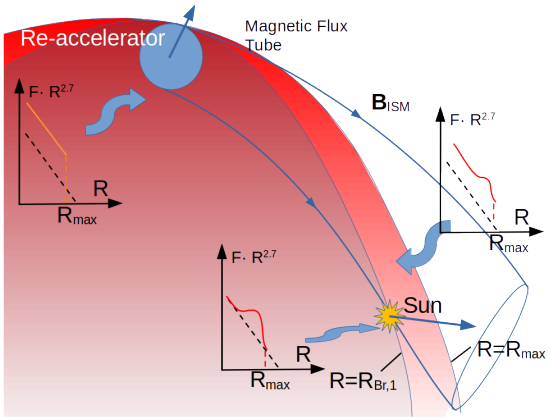

Figure 3: Schematics of a moving CR reaccelerator (e.g., a stellar bow shock–wind termination shock) and reaccelerated CRs that diffuse predominantly along the field lines, thus forming a wake behind this object. Three types of the reaccelerated CR spectrum are shown at different positions in the wake. Dashed black lines show the CR background spectrum, while the red lines show the spectrum of reaccelerated CRs at a given position in the stellar wake (see text).

The acceleration depends on the local shock angle: quasi-perpendicular shock ($\vartheta_{nB} \approx \pi/2$), vs. quasiparallel shock ($\vartheta_{nB} \ll 1$). A dull cone-shaped stellar bow shock makes a wide range of angles to the local field, $\vartheta_{nB} \leq \pi/2$, with a possible exception for $\vartheta_{nB} \ll 1$. Even a weak quasi-perpendicular shock ($\vartheta_{nB} \approx \pi/2$) of a size exceeding the particle Larmor orbit can provide the necessary energy upshift, operating in a shock-drift acceleration (**SDA**) regime. All it takes is that the shock overruns a significant portion of the particle's Larmor orbit before the particle escapes the shock front along the field line. A single full orbit crossing takes $r_g/U_{\rm shock}$ ≈30 yrs for $r_g \sim 3 \cdot 10^{15}$cm (a 10 TV proton in a 10 μG field) and $U_{\rm shock} \approx 30$ km/sec. Note that direct Voyager 1, 2 measurements give 7-8 μG just outside the heliosphere [11]. Stars with more powerful winds, such as the ϵ Eridani star discussed in [15], likely have a stronger field outside the astrosphere due to the Axford-Cranfield effect. It constitutes a magnetic pillow made of the stellar magnetic field blown out by the wind.

A turbulent wake flow reduces the field-aligned CR diffusion length to $\sim r_g\sqrt{c/U_{\rm shock}}$ [14] from the shock during the orbit crossing, assuming Bohm regime, $\kappa_\parallel = cr_g/3$. The particle energy gain after a single Larmor circle shock crossing can still be calculated from

the condition of adiabatic compression: $p_\perp^2/B = const$, where $p_\perp$ is the perpendicular to the magnetic field component of particle momentum. Therefore, even a factor of 2-3 shock (magnetic field B) compression would suffice to make the bump visible. The momentum gain should further increase by the Axford-Crandfield effect.

Consider an oblique portion of the bow shock to demonstrate the CR reacceleration. We will add to the standard DSA scheme [10] losses from the flux tube, important at higher rigidities, $R > R_L$. The result of reacceleration can then be cast as [15, 16]:

$$f_{\rm CR}\,(R) = A_b R^{-\gamma_b}\left\{1 + \frac{\gamma_b + 2}{q_s - \gamma_b}\exp\left[-\left(\frac{R_0}{R}\right)^a - \sqrt{\frac{R}{R_L}}\right]\right\} \tag{1}$$

Here $\gamma_b \approx 2.85$ and A_b are the *known* background CR index and normalization factor, respectively, q_s is the shock spectral index $q_s = (r+2)/(r-1)$, where r is the shock *unknown* compression, $R_0 \propto \left(L_s W/\sqrt{l_s}\right)^{1/a}$ is the characteristic bump rigidity that depends on the *unknown* distance to the shock, L_s, its size, l_s, and the level of turbulence in the flux tube, W. The **three** fundamental *unknown* bump-specific CR fitting parameters q_s, R_0, and R_L, can be obtained from fitting Eq.(1) to the proton spectrum (Fig.1), the best measured among CR species. *Therefore, our model needs only three parameters, which is two times less than the required minimal number of simple geometric parameters defining the bump shape, which is equal to* ***six****.* Moreover, as the spectrum is given in the element-invariant, rigidity form, the same fitting parameters derived from the proton spectrum can be used to predict the spectra of other elements, such as He, C, O, etc., and the secondaries with *no free parameters* [16]. These groups of CRs have their *fixed known* input parameters A_b and γ_b derived from their local ISM spectra below the bump, different from those of CR protons.

However, the most critical parameter for the fit is the turbulence-related index a: $W_k \propto k^{a-2}$, where W_k is the wave spectral density. For calculations shown in Fig.1, we have determined it from dimensional reasoning to be $a = 1/2$, which corresponds to the IK (Iroshnikov-Kraichnan) turbulence model, $k^{-3/2}$. Still, as we have used only three fitting parameters in Eq.(1) out of the six available, we can verify our calculation of a by minimizing the data mismatch. The mismatch has a very sharp minimum near $a = 1/2$ [15].

Moreover, the fit presented in Fig.1 for $a = 1/2$ rules out popular turbulence models other than IK. For instance, the Kolmogorov and Goldreich-Shridhar spectra do not fit the new high-fidelity data, shown in Fig.1. These spectra will likely dominate the ISM turbulence outside the flux tube. The fit does not call them into question since the IK spectrum is derived for a specific CR driver in the flux tube. Even more significant deviation from the data gives the Bohm turbulence regime, which, in turn, is expected closer to the shock that reaccelerates CRs but does not contribute to their propagation over the entire tube length. Our results thus point to the CR-filled flux tube (or its wake) as a set of choices for explaining the 10-TeV bump phenomenon. It most likely connects the Sun with a CR-reaccelerating shock 3-10 pc away.

Anisotropy If the shock is located at a few particle's mean free paths from the observer, a sharp increase in the CR intensity across the magnetic equator is expected and was indeed observed in [2], Fig.2 (right panel).

We use the Fokker-Planck equation for the CR propagation along the field [15]:

$$c\mu\frac{\partial f}{\partial \zeta}+\nu_{\perp}' f-\frac{\partial}{\partial \mu}\left(1-\mu^2\right)\mathcal{D}\left(p,\mu\right)\frac{\partial f}{\partial \mu}=Q\left(p,\mu\right)\delta\left(\zeta\right) \tag{2}$$

Here μ is the pitch angle cosine of a particle with momentum p. The spatial coordinate ζ is directed along the field, and the source is at the origin. The other two coordinates are removed by averaging the distribution function across the flux tube. The particle flux through its boundary enters as $\nu_{\perp}' f$ on the l.h.s. The CR scattering frequency $\mathcal{D}$ is related to the Alfven wave fluctuations E_k^A, by an IK spectrum. The solution is found by decomposing it in a series of eigenfunctions of the operator on its l.h.s. Starting from some distance from the source, it is dominated by the lowest eigenvalue $\lambda_0 \approx 2\sqrt{5\nu_{\perp}}$ and can be approximated near magnetic equator as $f_0 \approx \sqrt{5/\lambda_0}\left[1+\left(\lambda_0/4\right)|\mu|^{1/2}\,\mathrm{sgn}\mu\right]$, thus showing a sharp increase over the magnetic equator, consistent with the data presented in Fig.2 (right panel). Note that the Kolmogorov turbulence would produce a steeper rise of CR intensity across the magnetic equator, $\propto |\mu|^{1/3}\mathrm{sgn}\mu$, which might become discernible from the IK turbulence if the HAWC-IceCube statistics improve.

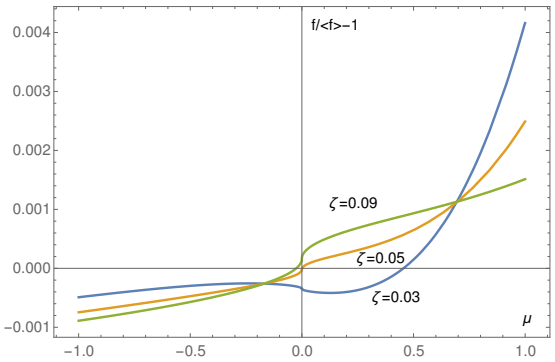

Figure 4: three solutions as a function of μ shown as a relative anisotropy, $\left(f-\langle f\rangle\right)/\langle f\rangle$. The isotropic part $\langle f\rangle \approx 0.50$ for all three values of ζ, and decreases with ζ insignificantly, since $\nu_{\perp}=10^{-6}$ and λ_0 ≈0.00447, $\lambda_1 \approx 45.0$, $\lambda_2 \approx 132$. The source anisotropy is $Q_1\left(\chi\right)=1+0.01\,|\chi|^3$ and eigenmodes decay with distance as $f_n \propto \exp\left(-\lambda_n|\zeta|\right)$.

The small-scale anisotropy ($f_{n\geq 1}$) can also be observed at the dimensionless distance to the source $\lambda_1|\zeta| \lesssim 1$. To illustrate the variation of small- and large-scale anisotropy with the distance, we show in Fig.4 the angular distributions of CRs at three different ζ. For ζ decreasing by a factor of 3, the CRs dipolar distribution shrinks to a sharp one toward the source. It shows a progressively stronger CR field alignment. Along with a jump across the magnetic equator at $\mu=0$, contained in f_0, an enhancement at $\mu \approx 1$, associated with f_1, is observed at the distances $0.05<\zeta<0.1$. This angular pattern can be found in Fig.2 (right panel). Its interpretation based on the ϵ-Eridani proximity naturally explains the puzzle of CRs predominantly arriving from the Galactic ANTI-center direction. At the same time, γ-ray observations of the diffuse emission by *Fermi*-LAT testify to a higher concentration of CRs in the inner Galaxy [4, 19] (see also Gabici's CRD Rapporteur1-01 talk). By contrast, even an advanced propagation model (Ivlev CRD6-05) based on distributed CR sources is unlikely to reproduce the sharp, especially Galactic anti-center prevalent CR anisotropy.

Gamma rays from ϵ Eridani Interestingly, there is an indication of the γ-ray emission in the direction of the proper motion of ϵ Eridani (RA: –974.758 mas/yr, Dec: 20.876 mas/yr [13]) at a distance of $\lesssim 0.5°$, which corresponds to the size of the astrosphere and the location of the bow shock. Fig.3 in [17] shows the position of ϵ Eridani with the white

circle in the middle of the $10^\circ \times 10^\circ$ region of interest. An excess emission to the right of the star (the direction of the proper motion) is marked with a green circle partially overlapping with the white circle, but the spectrum of the excess emission is not provided. The soft spectrum of the emission from *the star* may suggest background contamination rather than reflecting emission from the star itself. The authors of [17] speculate about the emission from interactions of cosmic rays with the debris disk around the star or the stellar activity. Unfortunately, the angular resolution of *Fermi*-LAT in the analyzed energy range 100 MeV – 3.16 GeV is rather poor and does not allow more details to be reconstructed.

Conclusions We have analyzed the high-fidelity data on the 10-TeV puzzling bump in the Galactic rigidity spectrum. It likely originates from 3-10 pc of the Sun. A system of bow + termination shocks associated with a star, such as ϵ-Eridani, especially if supplemented with its notably powerful stellar wind contribution to the CR reacceleration, may account for all observed bump features well within the data uncertainties with only three free parameters derived from a fit to the proton spectrum. A significant number of such features discussed make a coincidental agreement rather unlikely. Any combination of primary CR sources, such as SNRs, and variations in the CR propagation, cannot account for the fine angular and energy spectral structures. Their resulting CR spectrum would be smoother than observed since they operate over at least a few 100 pc scales.

Acknowledgments Work of MM, PD, and MC is supported by NSF grant AST-2109103, IM is partially supported by NASA grants 80NSSC23K0169 and 80NSSC22K0718.

References

[1] Abdo, A. A., Allen, B., et al., 2008. *Phys. Rev. Lett.*, 101(22):221101.
[2] Abeysekara, A., Alfaro, R., et al., 2019. *Astrophys. J.*, 871(1):96.
[3] Achterberg, A., Blandford, et al., 1994. *Astronomy and Astrophys.*, 281:220.
[4] Ackermann, M., Ajello, M., et al., 2012. *Astrophys. J.*, 750(1):3.
[5] Adriani, O., Akaike, Y., et al., 2019. *Phys. Rev. Lett.*, 122(18):181102.
[6] Adriani, O., Akaike, Y., et al., 2022. *Phys. Rev. Lett.*, 129:101102.
[7] Aguilar, M., Ali Cavasonza, L., et al., 2021. *Phys. Rep.*, 894:1.
[8] Amenomori, M., Bi, X. J., et al., 2017. *Astrophys. J.*, 836(2):153.
[9] An, Q., Asfandiyarov, R., et al., 2019. *Sci. Adv.*, 5(9).
[10] Blandford, R. D. and Ostriker, J. P., 1978. *Astrophys. J. Lett.*, 221:L29.
[11] Burlaga, L. F., Ness, N. F., et al., 2019. *Nature Astronomy*, 3:1007.
[12] Choi, G., Seo, E., et al., 2022. *Astrophys. J.*, 940(2):107.
[13] Gaia Collaboration, 2020. *VizieR Online Data Catalog*, I/350.
[14] Malkov, M. A., Diamond, P. H., et al., 2013. *Astrophys. J.*, 768:73.
[15] Malkov, M. A. and Moskalenko, I. V., 2021. *Astrophys. J.*, 911(2):151.
[16] Malkov, M. A. and Moskalenko, I. V., 2022. *Astrophys. J.*, 933(1):78.
[17] Riley, A. H., Strigari, L. E., et al., 2019. *Astrophys. J.*, 878(1):8.
[18] Skilling, J., 1975. *Mon. Not. R. Astron. Soc.*, 172:557.
[19] Zhang, R., Huang, X., et al., 2023. arXiv-2305.06948.